Interactions of same-row oxygen vacancies on rutile TiO_{2}(110)

B. B. Kappes, W. B. Maddox, D. P. Acharya, P. Sutter, and C. V. Ciobanu

The interactions of same-row oxygen vacancies on rutile TiO$_2$(110)

B. B. Kappes,[1] W. B. Maddox,[1] D. P. Acharya,[2] P. Sutter,[2] and C. V. Ciobanu[1*]

[1]*Division of Engineering, Colorado School of Mines, Golden, CO 80401*

[2]*Center for Functional Nanomaterials,*

Brookhaven National Laboratory, Upton, New York 11973

Abstract

Based on a dipolar-elastic model for oxygen vacancies on rutile (110), we evaluated analytically the overall energy of a periodic array of two vacancies and extracted the interaction parameters from total-energy density functional theory (DFT) calculations. Our calculations show that the dipole model holds for next-nearest neighbor vacancies and beyond. The elastic-dipolar interaction vanishes for adjacent vacancies, but they still experience an electrostatic repulsion. The proposed interaction model predicts a vacancy separation distribution that agrees well with that determined in our ultra-high vacuum scanning tunneling microscopy experiments, and provides a perspective for understanding earlier DFT reports.

Titanium dioxide –widely used in heterogeneous catalysis [1], photocatalysis [2], solar cells [3], or gas sensors [4], has become the prototype material for studying the reactivity of metal oxide surfaces [5]. Defects such as oxygen vacancies are always present on rutile surfaces [6] and, depending on their coverage and spatial distribution, can strongly influence the reactivity of the surface [7]. The interactions between vacancies determine their spatial distribution on the surface. Highly reactive vacancy clusters or pairs have not been expected to form because of vacancy repulsions [8], but recent experiments [9] do show the possibility of spontaneously formed oxygen vacancy pairs (OVPs), *i.e.,* of two adjacent vacancies in the same bridge-oxygen row. Regarding the stability of OVPs, early density functional theory (DFT) calculations came to contradictory conclusions: the OVPs were reported to have the highest [10] and the lowest [11] energy of all configurations of two vacancies per computational cell. A newer study [8] finds virtually the same energies for the OVP and the next-nearest neighbor (NNN) configurations, while another recent study [9] reports the NNN structure to have a much higher energy than the OVP. To date, several issues have prevented the complete, fundamental understanding of vacancy interactions, including their reliable quantitative determination; the more important ones are the difficulty of decoupling the interactions while using computational slabs of manageable size, and the sensitivity of various structural properties to the number of layers in the supercells [11, 12].

Here we show that the interaction of same-row vacancies on rutile (110) is dipolar-elastic in nature, with a long-range, inverse-cube dependence on their separation. This dipolar-elastic model holds when the vacancies are not adjacent, which we have found from DFT calculations at the level of the generalized-gradient approximation (GGA). Our approach has two key features that allow us to reliably determine the formation energies and the interaction parameters from total-energy GGA calculations: first, the interactions have been isolated to one bridge-oxygen row by using large supercells, and second, we have developed a closed-form expression for the overall interaction (per computational cell) associated with a periodic array of two vacancies. When vacancies are adjacent, they still repel, but this repulsion is much weaker than the dipolar-elastic one at the same distance. We have determined the distribution of vacancy separations (along bridge-oxygen rows) by scanning tunneling microscopy (STM), and have found that this distribution agrees well with that predicted from the calculated interactions. This validates our physical model for vacancy interactions, which we use to analyze our DFT data as well as data from other works [8, 9, 11].
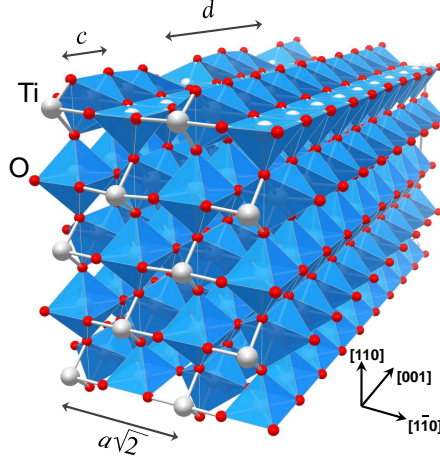
FIG. 1. (Color online) Reduced 10×2 rutile surface slab used in the DFT calculations. The interaction between the two bridge-oxygen vacancies is determined for different values of their separation d, $c \le d \le 5c$.

For the DFT simulations, we constructed 10×2, 600-atom stoichiometric supercells with dimensions $L_x = 2a\sqrt{2}$ and $L_y = 10c$ (with $a = 4.669$ Å, $c = 2.970$ Å [13]), and a thickness of five O-Ti-O trilayers. The vacancies were created by removing two same-row oxygen atoms spaced at d ($c \le d \le 5c$) [Fig. 1]. The DFT relaxations were carried out in the GGA framework using the PBE exchange-correlation functional [14], projector-augmented wave [15] pseudopotentials [16], and an on-site Hubbard term U for the Ti $3d$ states [17]. Charge neutrality ($Q = 0e$) was maintained for the stoichiometric slabs, but for the reduced slabs we also considered the positively-charged case ($Q = 4e$, corresponding to the removal of two O^{2-} ions). We have not searched for the localized electron configurations that most lower the total energy [18], but simply relaxed the structures from the bulk truncated positions and analyzed their final electronic structures. For our non-zero Hubbard term values, we have found that localization occurs on the same subsurface Ti atoms (in relation to the vacancies) for all spacings $d > c$; this finding justifies our analysis of the total supercell energy as a function of d, for each pair of (Q, U) values.

The difference ΔE between the total energy of the reduced slab (E_r) and the energy of the stoichiometric one of same area and thickness (E_s) can be written as

$$\Delta E \equiv E_r - E_s = 2(f - \mu_O) + w, \tag{1}$$

where f denotes the formation energy of a single vacancy (on an otherwise perfect and wide
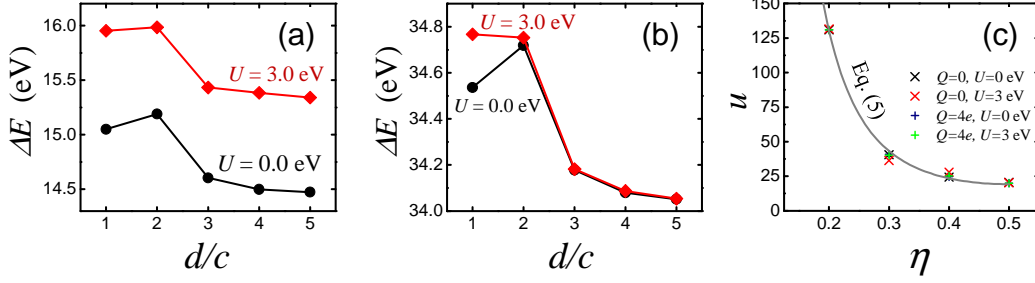
3

FIG. 2. (Color online) (a,b) The difference between the energy of a reduced (10×2) slab [(a) neutral, (b) positively charged] and that of a stoichiometric one. (c) Analytical dependence $u(\eta)$ (Eq. (5), curve) and numerical calculations of u for neutral ($\times$ symbols) and charged slabs ($+$ symbols).

surface), μ_O is the oxygen chemical potential, and w contains all interactions. Since we have collected all interactions into a single term w, which depends on the supercell dimensions and on the spacing between the vacancies, the formation energy f in Eq. (1) depends neither on the vacancy spacing between vacancies nor on their coverage. The variation of ΔE with the separation d at constant L_y ($L_y = 10c$) is plotted in Figs. 2(a,b) for neutral and positively charged slabs. In order to extract interaction parameters from ΔE vs. d data, we have to understand the overall interaction term w.

Therefore, we first focus on finding an analytic expression for w, and start by neglecting the cross-row interactions; this is reasonable given the large supercell dimension along $[1\bar{1}0]$, $L_x = 2a\sqrt{2} = 13.205$Å. In this approximation, w [Eq. (1)] depends only on the vacancy separation d and on the dimension L_y along a bridge-oxygen row. In the framework of elasticity theory, point defects on surfaces interact as elastic multipoles whose long-range interactions are inversely proportional to certain powers of their separation [19]. In what follows, we describe the interaction v between two *isolated* vacancies by the long-range dipolar-elastic repulsion

$$v(d) = \begin{cases} v_1 & \text{if } d = c \\ \frac{G}{d^3} & \text{if } d = ic, \ i = 2, 3, 4, ... \end{cases}, \tag{2}$$

where d is the distance between the two vacancies on an otherwise perfect surface, G is the strength of the dipolar repulsion, and v_1 is a short-range interaction present only for adjacent vacancies. When using periodic boundary conditions, the two vacancies are not isolated, since they interact with their periodic images as well. Using (2) for $d > c$ and collecting the

4

contributions from all periodic images along the same row, the total interaction energy per supercell can be written as a function of L_y and $\eta \equiv d/L_y$ via

$$w(L_y, \eta) = \frac{G}{L_y^3} u(\eta), \qquad (3)$$

with the function $u(\eta)$ given by

$$u(\eta) = \frac{1}{\eta^3} + \sum_{k=1}^{\infty} \left(\frac{2}{k^3} + \frac{1}{(k+\eta)^3} + \frac{1}{(k-\eta)^3} \right)$$
$$\equiv (1/\eta^3) + 2\zeta(3) - (\psi^{(2)}(\eta) + \psi^{(2)}(-\eta))/2 \qquad (4)$$

where ζ is the Riemann zeta function ($\zeta(3) \simeq 1.202$) and $\psi^{(2)}$ is the polygamma function of second order. Polygamma function identities [20] reduce Eq. (4) to

$$u(\eta) = 2\zeta(3) - \pi^3 \cot(\pi\eta) \csc^2(\pi\eta) - \psi^{(2)}(\eta). \qquad (5)$$

Eq. (5) is a general description of the interactions of two identical, elastically-repelling defects in the same row and their periodic images along that row; as such, it does not depend on the (common) type of the defects (*e.g.*, both vacancies or both adatoms), on their formation energy, or on their interaction strength.

TABLE I. Formation energies f ($= \overline{f} + \mu_O$), repulsion strengths G, and short-range interactions v_1 for different values of the slab charge Q and Hubbard parameter U. The standard deviations for $\overline{f}$ and f are the same.

$Q(e)$, U(eV)	$\overline{f}$(eV)	f(eV)	G(eVÅ^3)	v_1(eV)
0, 0.0	7.170 ± 0.006	2.244	169.8 ± 4.1	0.677 ± 0.013
0, 3.0	7.611 ± 0.013	2.684	152.0 ± 10.0	0.702 ± 0.027
4, 0.0	16.966 ± 0.004	10.207	157.7 ± 3.3	0.575 ± 0.009
4, 3.0	16.964 ± 0.006	10.205	165.1 ± 4.6	0.808 ± 0.013

Using Eqs. (1), (3), and (5), we fit the data in Figs. 2 (a,b) for $d \geq c$ to obtain the relative formation energies $\overline{f} \equiv f - \mu_O$ and the interaction strengths G for different Q (slab charge) and U (Hubbard parameter). The μ_O values [see Eq. (1)] that we have used were $\mu_O = -4.926$ eV (half the energy of an O_2 molecule) for the neutral system, and $\mu_O = -6.759$ eV (the energy of an isolated O^{2-} ion in the supercell) for $Q = 4e$. The calculated formation
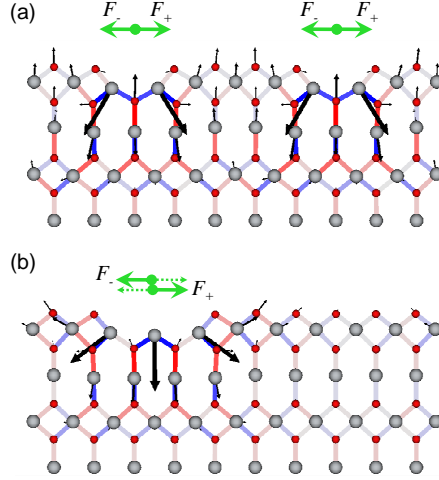
FIG. 3. (Color online) Displacement fields in a plane containing the vacancies separated by (a) $d = 5c$ and (b) $d = c$; for clarity, only three trilayers are shown. The green arrows show schematically the horizontal force dipoles associated with each vacancy (a), and illustrate the monopole cancelation responsible for the vanishing elastic repulsion at $d = c$ (b). The displacements (magnified here 10-fold for clarity) are calculated for the ($Q = 0e$, $U=0$eV) system with respect to the relaxed stoichiometric slab. The largest displacement magnitude is 0.41 Å in (a) and 0.44Å in (b).

energies and interaction strengths are listed in Table I for neutral and charged slabs at $U = 0.0$ eV and $U = 3.0$ eV. Using $\overline{f}$ and G values from Table I, we check our model by numerically calculating u from Eq. (1) [$i.e.$, $u = (\Delta E - 2\overline{f})L_y^3/G$ for $\eta \geq 2c/L_y$] and plotting it along with the analytic result Eq. (5). As seen in Fig. 2(c), the agreement between the numerical u values and the general formula Eq. (5) is very good, which validates a $posteriori$ our assumption that the interactions are reasonably well-confined to the bridge-oxygen row as long as the neighboring rows are defect-free.

Although multipole interactions between atomic-level defects (most often adatoms) on crystal surfaces have been reported [21], so far the particular dipolar-elastic model proposed here has not been proposed for oxygen vacancies. Figure 3(a) shows the atomic displacement fields and, schematically, the horizontal force dipoles (F_+, F_-) associated with each vacancy for $d = 5c$. The atoms located between vacancies experience opposite pulls resulting in an increase of energy, $i.e.$, the elastic repulsion. When the vacancies are brought close to form an OVP, there are no more 5-fold coordinated Ti atoms (5-f Ti) between them, which leads to the cancelation of two force monopoles as shown in Fig. 3(b). It may be worth noting

that monopole cancelation has also been evidenced as the origin of a short-range attraction that leads to step bunching on certain surfaces [22]. Despite this monopole cancelation, the interaction between vacancies at $d = c$ is not zero but a quantity v_1 [Eq. (2)] that can be found from a straightforward modification of Eq. (3),

$$w(L_y, \eta_1 \equiv \frac{c}{L_y}) = \frac{G}{L_y^3}u(\eta_1) - \frac{G}{c^3} + v_1. \tag{6}$$

Using Eqs. (1), (6) and the $\overline{f}$ and G values already calculated, we have found that the interaction v_1 is small but positive in all cases [Table I, last column]. This short-range repulsion is about one order of magnitude smaller than what the dipolar-elastic model would predict for vacancies at $d = c$ [$G/c^3 \approx 6.48$ eV], and is largely due to the electrostatic interactions of the exposed 4-f Ti with the nearby 5-f Ti atoms.

The directly observable manifestation of vacancy interactions is their spatial distribution, which we have analyzed from thermal vacancy populations. The samples were produced by Ar^+ sputtering cycles, followed by annealing the (110) rutile surface at a temperature $T = 950$ K, then rapidly cooling down to 77 K to freeze in the vacancy distribution. The vacancies were imaged using an ultrahigh vacuum (UHV, pressure below 10^{-11} Torr) cryogenic STM, in constant current mode with positive sample bias [23]. Vacancy separations were analyzed from portions of bridge-oxygen rows that had a vacancy concentration of $n \approx 15\%$. If there were no interactions, then a fixed vacancy coverage n would lead to an exponential decay of the probability to find vacancy-to-vacancy (V-V) segments of length d, $p_{nonint}(d) \propto \exp(-nd/c)$ [24]. Our data shows that $p(d)$ exhibits a maximum, and not the monotonic decay corresponding to the non-interacting system [green curve in Fig. 4]; this is a direct consequence of the repulsive interactions between vacancies.

In a canonical ensemble system of V-V segments, the interactions between the ends of segments give the single-particle energy levels $v(d)$ ($d = c, 2c, 3c, ...$) and thus a canonical distribution $p(d) = (1/Z) \exp(-nd/c) \exp(-v(d)/k_BT)$, in which Z is a normalization factor and k_B is Boltzmann's constant. The canonical distribution based on the interaction model Eq. (2) with the parameters in Table I is consistent with the experimental data [refer to Fig. 4], and is virtually the same for all (Q, U) pairs used in this study. The competition between the fixed coverage constraint and the rapidly-decreasing dipolar repulsion (G/d^3) gives rise to a most-probable vacancy spacing d^* which can be readily derived from the canonical distribution, $d^* = (3Gc/nk_BT)^{1/4}$. The G values (Table I) give d^* between $6.1c$
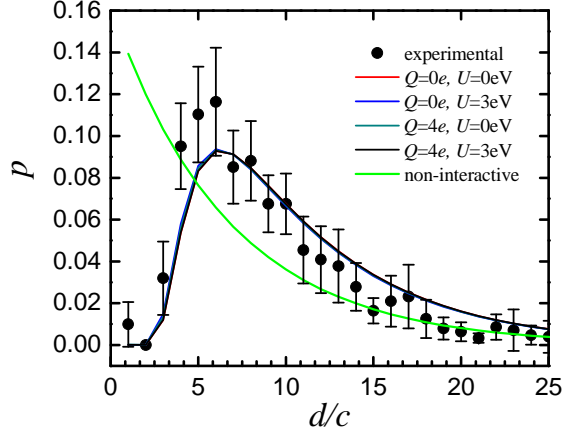
7

FIG. 4. (Color online) Distribution of vacancy spacings for $n = 15\%$ vacancy coverage at 950 K: STM experiments (dots with error bars) compared with the non-interacting system (exponential decay, green curve) and with the canonical distribution (four nearly overlapping curves). Note that the canonical distributions for different Q and U values are not fits to the experimental data, but are based on the interaction model Eq. (2) with the GGA values for G and v_1 listed Table I.

and $6.3c$, consistent with the experimental peak of $6c$. The agreement between the vacancy separation statistics determined in STM and the canonical distribution with GGA-calculated parameters validates our interaction model Eq. (2).

In the previous systematic attempts to compute the vacancy interactions on $TiO_2(110)$ [10, 11], the total energy was expressed as pairwise interactions from each vacancy to the next one along the row and also included cross-row couplings. Both reports [10, 11] acknowledged unresolved shortcomings of the pairwise model, which had manifested in significant differences of the total energies predicted by the model (with respect to those obtained directly from DFT calculations) once the model was applied to supercells other than those used to determine the pairwise interaction parameters. Departing from these pairwise models of Refs. [10, 11], we have proposed herein that the same-row vacancy interactions are dipolar, thus long-ranged. As we will show below, our model Eq. (3)–(6) holds very well when applied to different supercells (than those in Fig. 1), different numbers of vacancies (one or two) per cell, and different exchange-correlation functionals. For example, we have used Eqs. (3)–(6) and the $(Q = 0, U = 0)$ case data in Table I to compute the total energy difference between 5×3 supercells with two vacancies in the NNN and OVP configurations. We have obtained 0.264 eV, in excellent agreement with our GGA simulations performed

8

for 5×3 slabs, which place the NNN supercell energy at 0.249 eV above that of the OVP supercell; for the other three cases in Table I, the model [Eqs. (3)–(6)] yields total energy differences that are within 0.05 eV or less from the GGA results. Our results for 5×3 supercells are in disagreement (quantitatively) with the recently reported total energy difference of 0.8 eV [9], but based on our calculations and on the STM experiments that show similarly small occurrence probability for OVPs and NNNs (Fig. 4), we believe the 0.8 eV value to be in error.

Interestingly, data from other reports of DFT simulations [8, 11] can be readily understood using our model. The two-vacancy results in Ref. [8] ($c < d < 5c$) can be fitted well to our Eqs. (3), (5), yielding a strength $G = 244.9 \pm 7.9$ eVÅ^3 (not enough data is provided to determine f or $\overline{f}$). For one vacancy per supercell, the quantity denoted as VFE in [11] is defined as our $\Delta E \equiv E_r - E_s$ up to an additive μ_O. We find that the data for $p(m \times 1)$ cells ($m = 2, 3, 4, 6$) in table 2 of Ref. [11] fits closely our dipolar-elastic model, which for single-vacancy supercells takes the simple form $\Delta E + \mu_O = f + G\zeta(3)/L_y^3$. This data yields $f = 3.134 \pm 0.012$ eV and $G = 198.98 \pm 4.06$ eVÅ^3; these values are consistent with those in the first line of our Table I, but differ from them likely because of the thin slabs (and possibly other computational parameters) used in [11]. While we have devised our physical model for interactions confined to the same row, the structures in Refs. [8, 11] do not have any intact oxygen row and thus allow for cross-row coupling. Even so, the $p(m \times 1)$ data fits our elastic model very well, as judged by the small standard deviations obtained for f and G; in the case of Ref. [11] ($p(m \times 1)$ cells in table 2, $m \geq 2$), this is because at one vacancy per supercell, the cross-row interactions occur mostly perpendicular to the oxygen rows and thus amount to a constant independent of m (the cell dimension along the row). For the two-vacancy results in Ref. [8], the agreement with our model likely occurs because the diagonal cross-row interactions do not vary significantly as a function of d when $d > c$.

In conclusion, we have shown that the dipolar-elastic model describes well the long-range repulsion of same-row vacancies for all separations except $d = c$, where a much smaller short-range interaction is present. The model fits not only our DFT data, but explains several other results from the literature and gives an equilibrium vacancy separation distribution that agrees well with that determined in our STM experiments.

---

* Corresponding author, email: cciobanu@mines.edu

[1] J. A. Rodriguez *et al.*, Science **318**, 1757 (2007).

[2] A. L. Linsebigler *et al.*, Chem. Rev. **95**, 735 (1995).

[3] M. Gratzel, Nature **414**, 338 (2001).

[4] P. T. Moseley, Meas. Sci. Technol. **8**, 223 (1997).

[5] U. Diebold, Surf. Sci. Rep. **48**, 53 (2003).

[6] U. Diebold *et al.*, Surf. Sci. **411**, 137 (1998).

[7] R. Schaub *et al.*, Phys. Rev. Lett. **87**, 266104 (2001); O. Bikondoa *et al.*, Nat. Mater. **5**, 189 (2006); A. Tilloca *et al.*, J. Phys. Chem. B **109**, 20963 (2005). A. Tilloca and A. Selloni, ChemPhysChem **6**, 1911 (2005).

[8] Z. Zhang *et al.*, Phys. Rev. Lett. **99**, 126105 (2007).

[9] X. Cui *et al.*, J. Chem. Phys. **129**, 044703 (2008).

[10] A. Vijay *et al.*, J. Chem. Phys. **118**, 6536 (2003).

[11] M. D. Rasmussen *et al.*, J. Chem. Phys. **120**, 988 (2004).

[12] T. Brendow *et al.* Phys. Rev. B **70**, 035419 (2004).

[13] B.J. Morgan and G.W. Watson, Surf. Sci. **601**, 5034 (2007).

[14] J.P. Perdew *et al.*, Phys. Rev. Lett. **77**, 3865 (1996).

[15] G. Kresse, D. Joubert, Phys. Rev. B **59**, 1758 (1999).

[16] G. Kresse and J. Furthmüller, Comput. Mater. Sci. **6**, 15 (1996); *ibid.* Phys. Rev. B **54**, 11169 (1996). The bottom two trilayers were kept fixed, and the vacuum spacing was set to 12.0 Å. Spin-polarization was turned on, the plane wave energy cutoff was set to 400 eV, the Brillouin zone was sampled only at the Γ point, and the atomic coordinates were allowed to relax until the residual forces were smaller than 0.025 eV/Å. We used Gaussian smearing with a 0.05 eV width and dipole corrections along the surface normal to speed up convergence.

[17] S.L. Dudarev *et al.*, Phys. Rev. B **57**, 1505 (1998).

[18] N. A. Deskins *et al.* J. Phys. Chem. C **113**, 14 583 (2009); S. Chrétien and H. Metiu, *ibid,*

115, 4696 (2011).

[19] K.H. Lau and W. Kohn, Surf. Sci. **65**, 607 (1977); C. Teodosiu, *Elastic Models of Crystal Defects*, Springer-Verlag, Berlin (1982); J.M. Rickman and D.J. Srolovitz, Surf. Sci. **284**, 211 (1993).

[20] Eqs. 6.4.6-7 in M. Abramowitz and I.A. Stegun, *Handbook of Mathematical Functions*, Tenth Printing (1972).

[21] L.E. Shilkrot and D.J. Srolovitz, J. Mech. Phys. Solids **45**, 1861 (1997); P. Muller and A. Saul, Surf. Sci. Reps. **54**, 157 (2004); C.V. Ciobanu *et al.*, J. Eng. Mater. -T. ASME **127**, 462 (2005).

[22] C.V. Ciobanu *et al.*, Phys. Rev. B **68**, 201302 (2003).

[23] D.P. Acharya *et al.*, J. Phys. Chem. C **114**, 21510 (2010).

[24] The probability to encounter k vacancies in a row interval of length d is given by the Poisson distribution, $[(nd/c)^k \exp{(-nd/c)}]/k!$ [25]. For $k = 0$, this yields the probability to find uninterrupted segments of length d, $p_{nonint}(d) = (e^n - 1) \exp{(-nd/c)}$, after normalizing such that $\sum_{i=1}^{\infty} p(ic) = 1$.

[25] W. Feller, *An introduction to probability theory and its applications*, vol. I, 3rd edition (Sec. IV.6), Wiley & Sons, Inc. (1970).